

Off-Resonance Effects in Non-Conventional Spectroscopic Imaging

C. Schirda¹, and F. Boada²

¹Buffalo Neuroimaging Analysis Center, State University of New York at Buffalo, Buffalo, NY, United States, ²Radiology, University of Pittsburgh, Pittsburgh, PA, United States

Introduction: Fast spectroscopic imaging enables resolving the spectral information at much higher spatial resolutions compared to classical Chemical Shift Imaging (CSI) experiments, in shorter scan times. Besides fast CSI techniques that sample k-space on a Cartesian grid (e.g. Dixon), a number of non-conventional approaches employing non-Cartesian trajectories have been developed. Among them are stochastic trajectories [1], PREP [2], spiral [3] and rosette [4,5] trajectories. We theoretically analyze and experimentally demonstrate the off-resonance effects associated with these non-conventional encoding techniques.

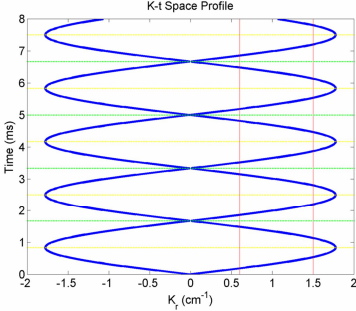


Figure 1: Rosette Trajectories k - t space profile through $k=0$ (blue). Yellow horiz lines-center of temporal slice (delimited by green lines). Vertic red lines – time axes at arbitrary distances from $k=0$.

Theory: While rosette trajectories [4,5] have the innate property of periodically sampling of center and edges of k -space, PREP and spirals achieve the same type of periodicity through gradient switching at $k=k_{max}$. The k - t space profile (Fig 1) parallel to the time axis, through $k=0$, reveals that each k -space location (in the sense of grid cell) is sampled in a regular fashion during the readout. Neglecting the T_2^* relaxation and assuming that the sampled signal within a grid cell $\alpha = (k_x \pm dk / 2, k_y \pm dk / 2)$ has a magnitude A_α and a phase φ_α at $t=0$, with $dk = 1 / fov$, the total off-resonance ω signal accumulated over the entire acquisition in that cell can be written as:

$$S_\alpha = \sum_{j=1}^{2 \cdot N_\delta} A_\alpha \cdot e^{i \cdot \varphi_\alpha} \cdot e^{i \cdot \omega \cdot t_\alpha^{(j)}} = \sum_{j=1}^{N_\delta} A_\alpha \cdot e^{i \cdot \varphi_\alpha} \cdot e^{i \cdot \omega \cdot t_\alpha^{(j-)}} + \sum_{j=1}^{N_\delta} A_\alpha \cdot e^{i \cdot \varphi_\alpha} \cdot e^{i \cdot \omega \cdot t_\alpha^{(j+)}} \quad (1)$$

Here $j \cdot \Delta t_\delta$ ($j = 0, 1, \dots, N_\delta$) are the times when the trajectories cross $k=0$ (which define N_δ temporal slices),

$(j-1) \cdot \Delta t_\delta + \Delta t_\delta / 2$ ($j = 1, \dots, N_\delta$) are the time positions of the median lines through these slices and $j \pm$ are the summation indices for data above and below these median lines. Using this notation, the distance in time between the data sampled at t_α and the closest median line is Δt_α . Then, for a given k -space location α , the time interval Δt_α is

the same in each temporal slice. Thus, the sampling times can be written as $t_\alpha^{(j\pm)} = (j-1) \cdot \Delta t_\delta + \Delta t_\delta / 2 \pm \Delta t_\alpha$, with

$\Delta t_\alpha = 1 / \Delta \delta$ the spectral dwell time (time separation between successive $k=0$ crossings). Equation (1) becomes:

$$S_\alpha = A_\alpha \cdot e^{i \cdot \varphi_\alpha} \cdot \cos(\omega \cdot \Delta t_\alpha) \cdot \frac{i \cdot (1 - e^{i \cdot \omega \cdot N_\delta \cdot \Delta t_\delta})}{\sin(\omega \cdot \Delta t_\delta / 2)} \quad (2)$$

The contribution of slow varying $\cos(\omega \cdot \Delta t_\alpha)$ term in (2) is less visible in the final image compared to the $1/\sin$ or faster varying exponential term and the magnitude of the normalized (to $f(0)$) spectral response function can be written as:

$$|f_N(\omega)| = \frac{1}{N_\delta} \cdot \left| \frac{\sin(\omega \cdot N_\delta \cdot \Delta t_\delta / 2)}{\sin(\omega \cdot \Delta t_\delta / 2)} \right| \quad (3)$$

T_2^* can be accounted for using $\omega \rightarrow \omega + i / T_2^*$. When using stochastic trajectories, the blue profile in Fig 1 cannot be represented as a solid line anymore, since the k -space locations will be irregularly sampled in time, and most of the summation terms in Eq (1) will be zero, resulting in the background noise observed in [1] and [4].

Methods: A multi-compartment oil-water phantom was scanned on a whole body 1.5T GE scanner, using the built in body coil. We chose the rosette trajectories since they have been demonstrated for both, a stochastic encoding scheme [4] and using a full spectral-spatial encoding approach [5]. The same gradient waveform was used for the two types of acquisition. Trajectories were designed [5] for a FOV=48cm, matrix size $N_x=160$,

$T_{read}=65ms$, $N_\delta = 28$, spectral bandwidth $\Delta \delta = 430Hz$, $T_R=100ms$. For the full k - t space encoding approach, $N_{sh}=196$ shots

were used with no averages (NEX=1), while for the stochastic approach $N_{sh}=9$ were used (to provide proper k_x - k_y coverage, determined using a simulation program) and NEX=22 averages, for a matched total scan time of 20 seconds.

Results: The fat and water reconstructed images for the stochastic and full encoding approach are shown in Fig 2. No filters were applied. For the full encoding approach, images were also reconstructed using only the data collected during the first half of the readout ($T_{read}/2$) corresponding to $N_\delta = 14$. In Fig 3, for the water profiles, it can be seen that the off-resonance fat contribution is approx. twice as large for the half readout (green) vs. the full readout (red line).

Conclusions: We showed that the spectral response function for spectroscopic imaging with self-rewinding trajectories is approximately equal to the PSF of the FT (Eq. 3). While stochastic encoding schemes can provide for significant speed advantages, the irregular sampling associated with them results in off-resonance signal showing as background noise on-resonance. The regular sampling in time associated with full spatial-spectral encoding results in incomplete suppression of image structure at off-resonance frequencies for shorter readouts (small N_δ). However, at $N_\delta = 32$ this effect is ~3-4%, while at $N_\delta = 64$ it is about 1-2% when $\Delta \delta$ twice the separation of the two resonances resolved.

References: [1] Scheffler, MRM 35(4), '96. [2] Mansfield, MRM 1(3), '84. [3] Meyer, MRM 28, '92 [4] Noll, IEEE Trans, 16(4), '97 [5] Schirda, Univ. of Pittsburg, PhD Dissertation, '07

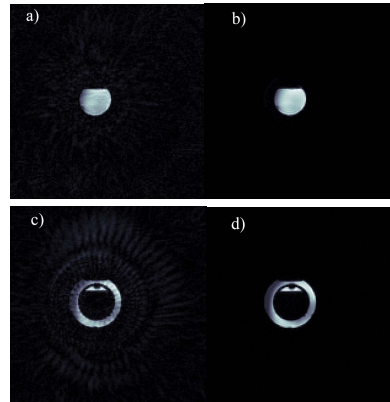


Fig 2: Stochastic (left) and fully encoded (right) images. Water(top) and Fat (bottom).

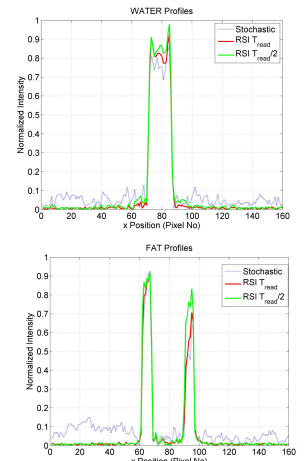


Figure 3: Center FOV horizontal profiles through water (top) and fat (bottom) images